Evaluating Rank-order Code Performance Using A Biologically-Derived Retinal Model

Basabdatta Sen and Steve Furber

***Abstract*— We propose a model of the primate retinal ganglion cell layout corresponding to the foveal-pit to test rank-order codes as a means of sensory information transmission in primate vision. We use the model for encoding images in rank-order. We observe that the model is functional only when the lateral inhibition technique is used to remove redundancy from the sampled data. Further, more than 80% of the input information can be decoded by the time only up to 10% of the ganglion cells of our model have fired their first spikes.**

I. Introduction

A Retinal model proposed by VanRullen and Thorpe has been shown to encode images in the rank-order of firing of the ganglion cells in such a way that a reconstruction using only 1% of the encoded data is recognisable [1]. This is consistent with the rank-order code hypothesis that offers an explanation of the near-instantaneous vision of the primate eye [2] [3]. Later, the information content of the decoded image was quantified using an objective metric of the perceptually-important information in the reconstructed image relative to the original image [4] [5]. Around 70% information retrieval was achieved by the time 20% of the ganglion cells in the retinal model had fired their first spikes. To further improve information recovery, different methods of rank-order decoding [6] and encoding [7] [8] using the retinal model were suggested.

However, this model is a coarse approximation to the different size and density of ganglion cells found in the primate retina. Ganglion cell parameters such as size and density are found to change considerably as a function of retinal eccentricity [9] [10] [11]. Moreover, it is understood now that there are at least fifteen [12] [13] different types of ganglion cell populating the primate retina with varying density depending on the function of each type. The most distinctive feature of the primate retina is the very high spatial density of the two principal varieties of ganglion cell, the midget and parasol cells, which constitute 80% and 10% respectively of the total ganglion cell population [9]. ON-centre and OFF-centre cells of each variety arborise in four independent layers [12]. This is significantly fewer than the sixteen layers used in VanRullen and Thorpe's retinal model (referred to hereafter as VR & T's retinal model), the layered structure being dyadic in nature. Moreover, ON-centre and OFF-centre cells of either variety at a certain spatial location in the primate retina differ in size and sample the image independently [9]. Again, this is unlike VR & T's retinal model where, at a certain spatial location, either an ON- or an OFF-centre cell fires in response to a stimulus, but never both because, having the same receptive field, only one of the two can have a net positive input. Thus, a retinal model with cell parameters and layout emulating those found within a smaller eccentricity in biology is desirable in the study and analysis of neural encoding in the early visual pathway. The goal of this work is to develop such a model and subsequently use it for rank-order encoding images.

It is said that "a precise description of foveal geometry is the keystone of any good model of primate retinal topography" [14]. The area in the primate V1 representing the fovea has greater spatial resolution by a factor of more than 1000 than that representing the peripheral retina [9] [15] [16]. The foveal pit is a circular region of about $200\mu m$ diameter at the centre of the primate retina [17]. The only photoreceptors available here are the cones, the connected neurons being displaced radially outwards [14]. Such an arrangement provides direct access of incoming light to the cones, making the foveal-pit the region of highest visual acuity. Retinal ganglion cell sizes in each layer increase the further they are from the centre of the fovea [10]. A model based on cell parameters within a small foveal eccentricity thus gives a model of the highest resolution region of the visual field. Furthermore, the displaced amacrine cell count is observed to be close to zero in regions close to the foveal centre [15], which reduces errors in ganglion cell count subserved by foveal cones.

In this work, we develop and simulate a model of ganglion cell layers within a small eccentricity of the retinal foveal-pit of primates and use it for rank-order encoding images as was done using VR & T's retinal model. We observe that a Filter-overlap Correction algorithm (FoCal) based on lateral inhibition [8], a technique used by sensory neurons to remove redundancy from incoming information, is vital to the working of the foveal-pit model. This reflects the dependency of retinal neurons on lateral inhibitory circuits for proper functioning. We observe that on average more than 85% of the perceptually-important information contained in the input stimulus can be recovered in reconstructed images. Moreover, this information is retrieved by the time only up to 20% of the cells in the foveal-pit model have fired their first spikes. This is an improved performance compared to an average of 70% information retrieval by the time 20% of the ganglion cells in VR & T's retinal model fire [4]. We

Steve Furber is ICL Professor of Computer Engineering at the School of Computer Science, University of Manchester, UK (email: steve.furber@manchester.ac.uk). Basabdatta Sen Bhattacharya has been a PhD student working with Prof. Furber at the School of Computer Science, University of Manchester, UK from 2004 to 2008 (email: basab815@gmail.com).

Steve Furber is supported by a Royal Society-Wolfson Research Merit Award.

978-1-4244-3553-1/09/$25.00 ©2009 IEEE

therefore claim that rank-order codes perform even better with the foveal-pit model.

The outline of the paper is as follows: We present the biological background and structure of the foveal-pit model in Section II. In Section III we discuss the rank-order encoding of images using the foveal-pit model and show that FoCal is vital to the performance of the model. In Section IV we present a qualitative and quantitative evaluation of the perceptually-important information preserved in images reconstructed from rank-order encoded data obtained using our model. We present our conclusions and suggestions for further work in Section V.

II. A MODEL OF THE FOVEAL-PIT

A. Biological basis of the model

- *Model eccentricity*: The primate foveal cones are arranged in a very dense and fairly regular triangular mosaic with the maximum density and smallest sizes found in the foveal pit region, the density decreasing by around 50% at a radial distance of $100\mu m$ [10]. We consider a sampling window of radius $50\mu m$ at or near the foveal centre, which contains around 1500 cones [14] with a minimum centre-to-centre spacing of $2.8 - 3\mu m$ [18]. We design our model based on the characteristics of the foveal cones and their subserved ganglion cells within this window. The midget and parasol ganglion cells together constitute 90% of the ganglion cells in the primate retina [19]. Moreover, in the foveal region the population of midget ganglion cells is observed to be around 95% of the total ganglion cell population [11]. We find a lack of quantified information about the exact proportions of other types of ganglion cell in the primate foveal region [12]. We therefore consider only midget and parasol ganglion cells in our model.
- *Ganglion cell to cone ratio*: The radial displacement of the ganglion cells subserved by the foveal cones is an obstacle to the exact tracing of synaptic wiring between the two classes of neurons in the primate fovea [20]. Cumulative analysis shows the ganglion-cell-to-cone-count ratio within the primate fovea to be $3.34 - 4 : 1$, with a possibility of being greater than $4 : 1$ at the centre of the fovea [14]. Elsewhere this range is specified as $2.7 - 3.4 : 1$ [21]. We employ a ratio of $4 : 1$ in our model.
- *Ganglion cell size and layout*: The mosaics of the ON- and OFF-centre midget and parasol cells are independent of each other [9]. On average, the dendritic field diameter of an ON-centre ganglion cell is 30% greater than that of its OFF-centre counterpart across all eccentricities in the retina [19] [11]. Adjacent midget cell dendritic trees in each layer abut one another but show very little overlap [11]. Parasol cell dendritic trees show a larger overlap, with a coverage factor[1] observed at 3.4 [19] compared to 1 for midget cells [23]. In the central retina, human midget cells outnumber parasol cells by around $30 : 1$ [19]. Midget cells in the central retina have a diameter $\simeq 5 - 9\mu m$ [11] [23], and the ratio of the dendritic tree diameter of a parasol cell to that of a midget cell of each type is found to be around $10 : 1$ [19].
- *Ganglion cell receptive field size*: The receptive field centre (RFC) diameter of a ganglion cell is on average 1.65 times larger than that of its dendritic tree in the foveal region [24]. This difference is due to the convergence of signals from other neurons onto the pathway from the cones to the ganglion cells and is at a maximum near the fovea [24].The surround of a midget cell receptive field is on average 6.7 times wider than its centre, while that of a parasol cell is 4.8 times wider than its centre [24].

[1]defined as 'dendritic field area $\times$ cell density' [22]

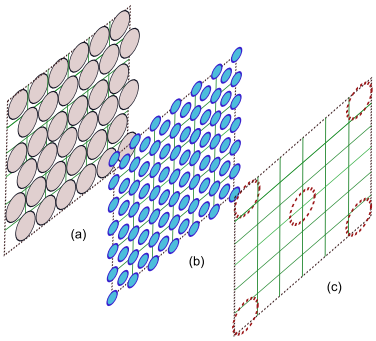

Fig. 1. (a) Hexagonal cone lattice mapped on a digital raster. (b) The midget ganglion cells and (c) parasol ganglion cells mapped on the raster in triangular lattice. Intercell spacing is $1/\sqrt{2}$ pixel for midget cells and $5/\sqrt{2}$ pixel for parasol cells.

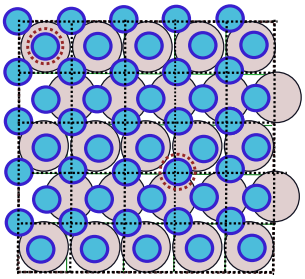

Fig. 2. The layout of the midget and parasol ganglion cells on a 5×5 region of the raster shown in Fig. 1. The OFF-centre ganglion cells of each variety are shown here. The ON-centre cells of both midget and parasol variety are equal in number to their respective OFF-centre counterparts. Thus, the 5×5 region of the raster shown here has a ganglion-cell-to-cone count ratio of $\approx 4 : 1$ as observed in primate fovea.

B. Designing the model

We consider a cone layer arranged in a hexagonal lattice and projected on a digital raster as shown in Fig. 1(a). We presume the subserved ganglion cell layers to be directly beneath the cone layer, instead of being laterally shifted, as the latter does not have any functional implication in our model. The midget and parasol OFF-centre cells subserved by the cone layer are arranged on a triangular lattice on this raster, as shown in Fig. 1(b) and Fig. 1(c) respectively, for

consistency with the biological layout of the cells and to maintain the ganglion-cell-to-cone-count ratio as observed in biology. For a 5×5 pixel region on the raster shown in Fig. 2, there are 25 cones, 50 midget OFF-centre cells and 2 parasol OFF-centre cells. The ON-centre cells for each variety of ganglion cell are observed to have a lower spatial resolution than their OFF-centre counterparts due to their larger sizes [11] [23]. However, due to the very high density of cells in the foveal region, this difference is negligible for all practical purposes. Thus, we consider a similar spatial resolution of ON- and OFF-centre cells of each variety in our model. Therefore, the total counts of midget and parasol cells are 100 and 4 respectively against a cone count of 25 in Fig. 2. The ganglion-cell-to-cone-count ratio in our model is thus $\approx 4:1$ as observed in the primate retina. Furthermore, midget cells constitute $\approx 96\%$ of the ganglion cell population in our model, while the midget-to-parasol-count ratio is $25:1$, both of which are close to their respective observed figures of 95% and $30:1$ in biology.

TABLE I

TABLE SHOWING THE VARIOUS PARAMETERS AND THEIR SPECIFICATIONS FOR SIMULATING GANGLION CELL RECEPTIVE FIELDS OF THE FOVEAL-PIT MODEL.

Ganglion Cell Types		Receptive Field Simulation Parameters				
		matrix size (n)	std. dev. centre (σ_c)	centre width in pixels (w_c)	std. dev. surround (σ_s)	sampling resolution
midget	OFF-centre	5×5	0.8	3	$6.7 \times \sigma_c$	$\frac{1}{\sqrt{2}}$
	ON-centre	11×11	1.04 $\simeq (1.3 \times 0.8)$	5		
parasol	OFF-centre	61×61	8 $\simeq (10 \times 0.8)$	33	$4.8 \times \sigma_c$	$\frac{5}{\sqrt{2}}$
	ON-centre	243×243	10.4 $\simeq (10 \times 1.04)$	53		

The centre-surround structures of ganglion cell receptive fields are simulated with Difference of Gaussian (DoG) functions and are defined as: $\Phi(\mathbf{x}) = \pm\frac{1}{2\pi\sigma_c^2} exp\left[\frac{-\|\mathbf{x}\|^2}{2\sigma_c^2}\right] \mp \frac{1}{2\pi\sigma_s^2} exp\left[\frac{-\|\mathbf{x}\|^2}{2\sigma_s^2}\right]$, where σ_c is the centre width, σ_s is the surround width, and $\pi\sigma_c^2$ and $\pi\sigma_s^2$ are used for normalisation [25] [1]. The midget OFF-centre cell receptive field is simulated with a 5×5 DoG where $\sigma_c = 0.8$, so that the RFC diameter for midget OFF-centre cells is $w_c = 3$ pixels. As mentioned in Section II-A, the dendritic tree of an ON-centre ganglion cell in the primate retina is observed to be 30% larger than that of its OFF-centre counterpart. Again, the RFC width of all midget cells in the foveal region is 1.65 times larger than that of their respective dendritic trees. Thus, we can say that the RFC of an ON-centre midget cell is 30% larger than that of its OFF-centre counterpart. The RFC width of the midget ON-centre cells in our model is thus set as $\sigma_c = 1.04$. The receptive field surround width for both the ON- and OFF-centre midget cells, σ_s, is taken as 6.7 times that of their respective RFC width as found in biology. Table I shows the various parameters that we use in simulating the ganglion cell receptive fields in the foveal-pit model. The matrix sizes representing the DoGs corresponding to each variety and type of ganglion cell are adjusted so as to conform to biological specifications while being computationally convenient. The RFC width of the parasol OFF- and ON-centre cells is set to 10 times that of their respective midget cell counterparts, while the width of receptive field surround is taken as 4.8 times that of the RFC, as in biology.

III. THE FOVEAL-PIT MODEL AS A RANK-ORDER ENCODER

An $M \times M$ image $\mathcal{I}$ is filtered by DoG functions with matrix size and sampling resolution as shown in Table I. This generates an array C_{nor} consisting of a total of T coefficients-of-filtering, where $C_{nor} = \langle \Phi(\mathbf{x}), \mathcal{I} \rangle$ and $T \approx 4.16M^2$. As each DoG represents a ganglion cell, the image can be thought of as being processed by a total of T ganglion cells. The magnitude of each coefficient $c_{j,k}^{nor} \in C_{nor}$ represents the strength of activation of a ganglion cell produced by the contrast at spatial location (j,k) in the image $\mathcal{I}$. The relative magnitude of a coefficient simulates the latency of its firing in a population of ganglion cells. Thus, the larger of two coefficients corresponds to a ganglion cell which fires earlier than the cell corresponding to the smaller coefficient. Rank-order encoding of spikes is simulated by sorting C_{nor} to obtain $\{c_i \in C_{or} : c_i > c_{i+1} \forall i = 1 \cdots T\}$ [1] [4]. The rank-ordered coefficients in C_{or} represent the image $\mathcal{I}$ encoded in the latency of each incoming spike from a population of asynchronously firing ganglion cells. These coefficients are then used for rank-order decoding to obtain a reconstructed image: $\mathcal{I}_{rec} = \langle \Phi(\mathbf{x}), C_{or} \rangle$ [1] [4] [6]. This method of rank-order decoding assumes DoG orthogonality where $\langle \Phi_i(\mathbf{x}), \Phi_{i+1}(\mathbf{x}) \rangle \approx 0$. However, neighbouring RFCs, as observed in primate retina, are very much overlapping. Thus they cannot be presumed to be approximately orthogonal as was done in VR & T's retinal model [1] [7]. This anomaly is reflected in the reconstructed image shown in Fig. 3(b). In [4], we introduced an objective metric Q to obtain a quantitative measure of information recovery from rank-order encoded images. The metric was originally proposed in the image fusion domain and measures perceptually-important information preserved in fused images in terms of accuracy in transfer of local gradient information from the original images [5]. Furthermore, the metric is parametrised with extensive subjective evaluation [26] and modulated according to the non-linear contrast sensitivity of the human visual system. We use Q, as well as Root Mean Square Error (RMSE), a measure which is commonly used as an image quality metric, to quantify and compare the original and reconstructed image qualities. The Q and RMSE plots in Figures 3(e) and 3(f) for progressive build up of information during image reconstruction using each coefficient of the array C_{or} confirms the subjective impression given by Fig. 3(b).

Significant overlap between neighbouring RFCs gives rise to redundancy in the rank-order encoded image due to

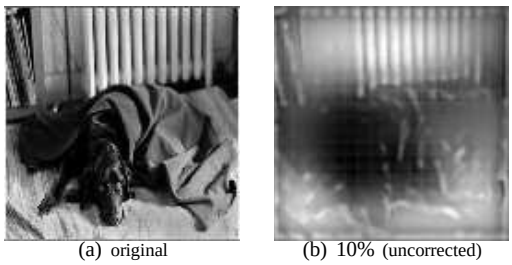

(a) original (b) 10% (uncorrected)

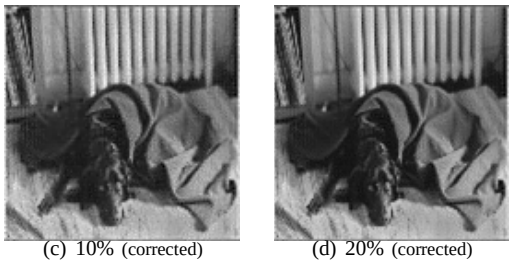

(c) 10% (corrected) (d) 20% (corrected)

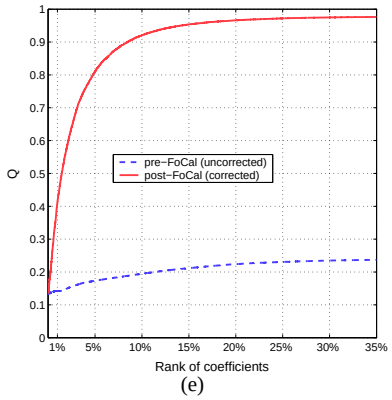

(e)

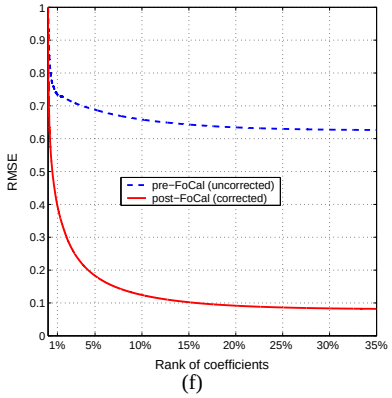

(f)

Fig. 3. (a) An input stimulus to the foveal-pit model. (b) Reconstruction with 10% of the rank-order encoded data with no correction for data redundancy. (c), (d) Reconstruction with 10% and 20% of the rank-order encoded data corrected using FoCal for information redundancy due to RFC overlap. (e) A comparison of the perceptually-important information recovery from data without and with redundancy removal using FoCal. (f) A comparison of the reconstructed image quality compared to the original using RMSE for images reconstructed from data without and with redundancy removal using FoCal.

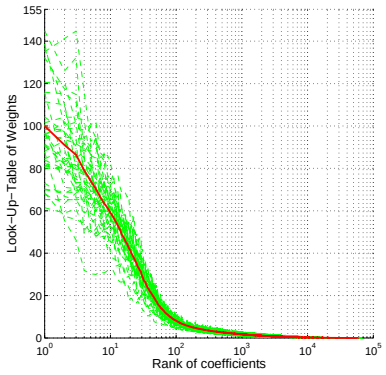

(a)

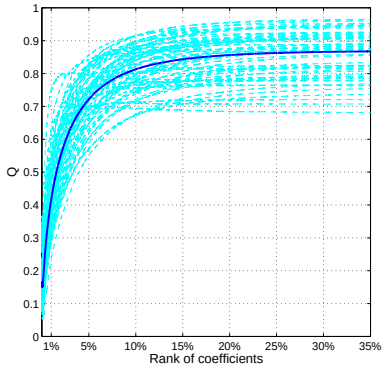

(b)

Fig. 4. (a) Look-Up-Table of weights for decoding images rank-order encoded using the foveal-pit model in conjunction with FoCal. (b) Perceptually-important information recovery plot for all sixty-five images in our data-set during progressive reconstruction using the LUT, shown as a spread about the mean information recovery plot.

an over-representation of a point in space. Interestingly, redundancy reduction has long since been described as a goal of sensory processing for efficient information transmission [27] [28] [29], and is thought to be dealt with in the primate retina using lateral inhibition [30] [31]: a mechanism where neighbouring neurons inhibit one another so as to optimise spatial representation. Moreover, the inhibitory effect of several neighbouring cells upon a certain cell is additive and is expressed quantitatively as [32]: $r_p = e_p - \sum_{j=1}^{n} K_{p,j}(r_j - r^0_{p,j})$, where $p = 1, 2, \ldots, n$, $j \neq p$, r_p is the firing frequency of a receptor unit p, e is the excitation supplied by the external stimulus on the receptor, $K_{p,j}$ is the coefficient of inhibitory influence of receptor unit j on p, r^0 is the threshold frequency that must be exceeded before one receptor can exert any inhibition on the other and $r_j \geq r^0_{p,j}$. Recently, we have used this relation to propose a Filter-overlap Correction algorithm (FoCal) [8]. We have used FoCal to optimise information recovery from rank-order encoded images using VR & T's retinal model [8]. In this work, we use FoCal to correct the high RFC overlap in the foveal-pit model.

We modify C_{or} using FoCal: every coefficient $\{c_p \in C_{or} \forall p\}$ corresponding to a DoG Φ_p is corrected for col-

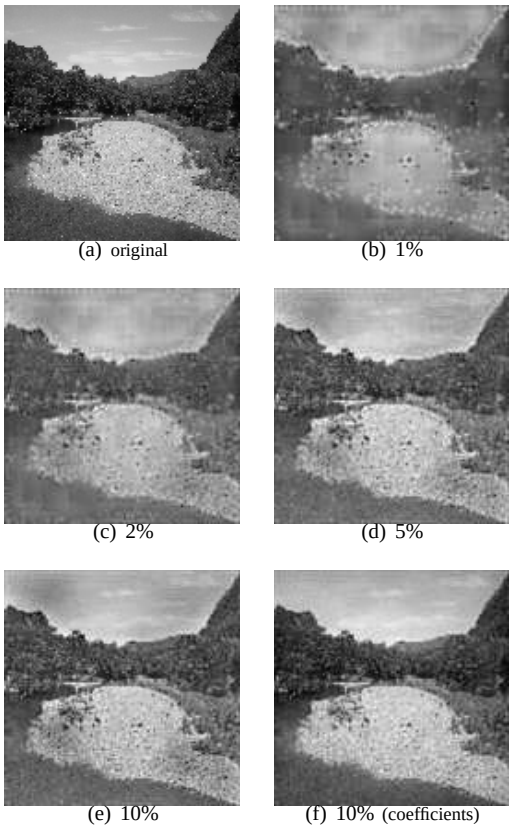

(a) original (b) 1% (c) 2% (d) 5% (e) 10% (f) 10% (coefficients)

Fig. 5. (b)–(e) The image in (a) reconstructed using up to 1%, 2%, 5% and 10% of the LUT weights. (f) Image reconstructed using 10% of its own coefficients-of-filtering. The loss during image reconstruction using LUT can be seen by comparing (e) and (f).

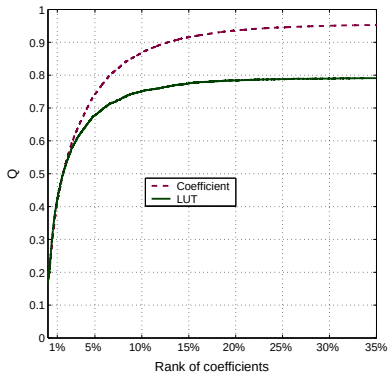

(a)

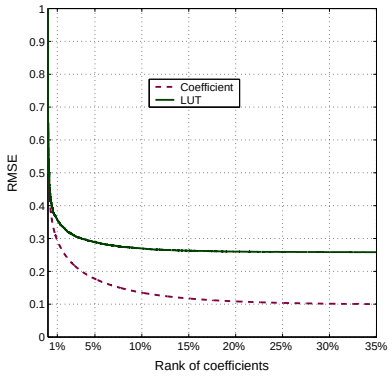

(b)

Fig. 6. (a) Perceptually-important information recovery plots for progressive reconstruction of the image shown in Fig. 5(a) using its own coefficients-of-filtering against LUT weights. (b) RMSE plots for the same.

lective overlap with neighbouring filters by $c_p = c_p - c_j.\langle \Phi_p, \Phi_j \rangle$ [8]. C_{or}, thus modified, is then re-ordered to obtain C_{or}^{mod}, which is now used to progressively reconstruct images. The difference in image quality between Figures 3(b) and 3(c) shows the role of FoCal in redundancy removal from rank-order encoded data. From the Q plot in Fig. 3(e), more than 90% of the perceptually-important information is seen to be recovered by the time around 20% of the coefficients are used for image reconstruction. This is also evident from a comparison of Figures 3(a) and 3(d). The RMSE plot in Fig. 3(f) is an alternative measure that confirms the trend shown in the Q plot.

IV. Results

We use a data-bank of 65 grayscale images of size 128×128 and consisting of natural and man-made structures. The images are filtered with the foveal-pit model, and the coefficients-of-filtering thus obtained are rank-order encoded applying FoCal. The sixty-five rank-ordered arrays are then averaged to obtain an array $\mathcal{R} = \frac{1}{K} \sum_{u=1}^{K} C_{or_u}^{mod}$, where u represents the u^{th} image in a data-set consisting of K images. Thus, $\mathcal{R}$ corresponds to a Look-Up-Table (LUT) of weights that is used to reconstruct a rank-order encoded image rather than C_{or}^{mod} corresponding to the image. This is same approach as was used to generate a LUT for VR & T's retinal model [1]. Thus, the first LUT weight corresponds to the ganglion cell which is the first in the population to fire a spike. Further, only the first spike of each cell is considered for rank-order encoding. Progressive reconstruction using $\mathcal{R}$ simulates information retrieval with each incoming spike fired by a ganglion cell at a certain spatial location in the foveal-pit model. The LUT for our foveal-pit model is shown in Fig. 4(a). The perceptually-important information recovery plots of all the images in our data-set using $\mathcal{R}$ are shown in Fig. 4(b) as a spread about the mean plot. We observe that on average around 85% of the perceptually-important information can be recovered from images rank-order encoded with the foveal-pit model using FoCal. Further, this information is recovered by the time around $15 - 20\%$ of the LUT weights are used for image reconstruction, with more than 80% of the available information already recovered by the time only around 10% of the ganglion cells have fired their first spikes. This is a remarkable improvement in the speed of information recovery compared to that displayed by VR & T's retinal model [4], and conforms very well to the main goal of rank-order encoding — fast information retrieval. We do a qualitative evaluation for an image from our data-set shown in Fig. 5(a). From Fig. 5(b), we observe that we can fairly decipher the contents and structure of the original image, thus demonstrating that a picture from our data-set is also

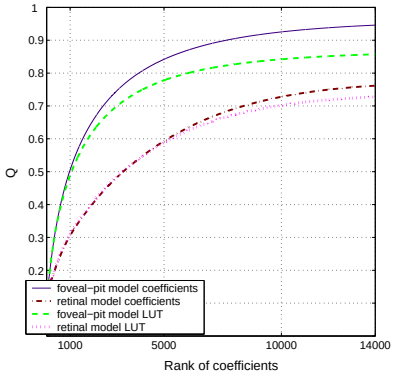

Fig. 7. Average perceptually-important information recovery plot using both the coefficients of filtering as well as the respective LUTs of the foveal-pit model and VR & T's retinal model. Progressive information recovery is measured in terms of the absolute number of rank-ordered coefficients or weights from the LUT used for reconstruction.

recognisable by the time only 1% of the LUT weights are used for reconstruction. Moreover, we observe that except for edge enhancement, there is no extra information about the scene in Fig. 5(e) as compared to Fig. 5(d). Thus, all the vital information about the scene seems to be present in the reconstruction in Fig. 5(d) using 5% of the LUT weights, which contains 70% of the perceptually-important information as can be seen in Fig. 6(a). Deterioration in information recovery and image quality due to reconstruction using approximate data in $\mathcal{R}$ as compared to exact data in C_{or}^{mod} for an image is also shown in Figures 6(a) and 6(b), while Figures 5(e) and 5(f) are provided for subjective evaluation of the same.

Due to a coarser sampling resolution used in VR & T's retinal model, the total number of coefficients of filtering in the model $T' \approx 2.67M^2$, which is approximately 50% less than T as defined in Sec. III. Thus, one might argue that a one-to-one comparison of information recovery using the two models against their respective percentage of coefficients may not be appropriate. In Fig. 7, we present a comparison of the information recovery for both the models against the number of coefficients used in progressive information recovery rather than the percentage. Average information recovery plots for progressive reconstruction using both the true coefficients of filtering of the images as well as the LUTs of the respective models are shown. The results show a significant improvement in both the quantity as well as rate of information recovery obtained using the foveal-pit model.

To complete the preliminary testing of the foveal-pit model as a rank-order encoder, we present our model with three images shown in Figures 8(a) – 8(c) which were not a part of our data-set of 65 images used to generate the LUT. We choose these out-of-sample images so as to include text as in Fig. 8(a), a man-made structure as in Fig. 8(b) and a natural scene as in Fig. 8(c). We show the respective reconstructed images using up to 10% of the weights from $\mathcal{R}$ in Figures 8(d) – 8(f). The perceptually-important information recovery plots for progressive reconstruction using

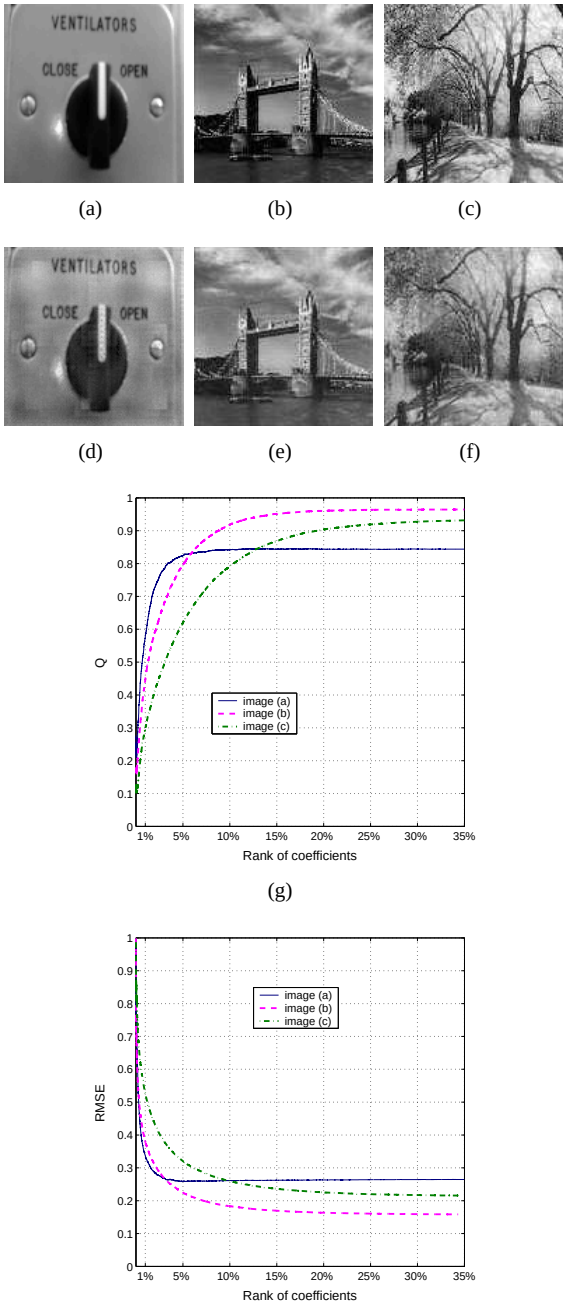

Fig. 8. (a–c) Three images which are not a part of the data-set of sixty-five images used to generate $\mathcal{R}$, the LUT for the foveal model. (d–f) Images in (a–c) respectively reconstructed using the first 10% of the LUT values. (g) The perceptually-important information recovery plots and (h) RMSE plots during progressive reconstruction of the images.

$\mathcal{R}$ for each of the three images are shown in Fig. 8(g). We observe that around $85-90\%$ of the available information is recovered from the rank-order encoded data for all the three images, and that almost all of this information is recovered by the time only around 20% of the ganglion cells have fired their first spikes. Further, around 80% or more information is retrieved by the time around 10% of the ganglion cells have fired their first spikes. The corresponding RMSE plots are also shown in Fig. 8(h). Thus, the foveal-pit model is shown to perform efficiently with out-of-sample data.

V. Discussion and further work

In this work, we have designed a model of the foveal-pit ganglion cells with the aim of moving an existing retinal model closer to biology. By so doing, we have developed a 'shallow' but densely packed model which resembles the retina more closely than a 'deep' and sparse model such as VR & T's [1]. We showed that the role of FoCal (Filter-overlap Correction algorithm [8]) is critical for rank-order encoding using the foveal-pit model in order to deal with RFC overlap; this is similar to the lateral inhibition mechanism used by sensory neurons to deal with data redundancy introduced due to oversampling by the overlapping ganglion cell receptive fields. We also showed that the foveal-pit model is highly efficient in preserving information about an input stimulus during rank-order encoding; around 80% of the information is available by the time only up to 10% of the ganglion cells of the model have fired their first spikes, while vital aspects of the encoded information have already been retrieved with only the first 5% of the ganglion cells firing. We claim that rank-order codes perform better using a biologically-derived retinal model. Again, the foveal-pit model as well as VR & T's retinal model are not simulated in real time; rather, spike latencies are being simulated with a table of average weights. Moreover, the interneurons in the pre-ganglion retinal layers play a crucial role in processing the sampled data and in information transmission pre-spiking. These aspects are to be considered in future work as an enhancement to the model. We expect that with only 4 layers of ganglion cell in the foveal-pit model, information loss during data-processing will be less for real-time implementation as compared to VR & T's retinal model with its 16 layers.

The model is a promising basis for further empirical studies of information processing in the retina. One such application would be to use the model for simulating dynamic scene perception using eye saccades, the sole purpose of which is to project a point of interest onto the fovea. The model can also be used to evaluate other proposed neural encoding mechanisms, as a basis for comparison with rank-order codes. An obvious extension to the model is to study colour vision with foveal cones, and related information recovery, which is yet to be investigated with rank-order codes. Furthermore, FoCal introduces lateral inhibition in the model post-spiking whereas the biological system employs lateral inhibition in the non-spiking neurons that precede the spiking ganglion cells in the sensory information flow. It is likely that pre-spiking lateral inhibition can support even better information redundancy removal than we have shown in our model.

References

[1] R. VanRullen & S. Thorpe, "Rate coding versus temporal order coding: what the retinal ganglion cells tell the visual cortex,"*Neural Computation*, vol. 13, pp. 1255-1283, 2001.

[2] S. Thorpe et al., "Speed of processing in human visual system," *Nature*, vol. 381, pp. 520-522, 1996.

[3] S. Thorpe & J. Gautrais, "Rank order coding," *Computational Neuroscience: Trends in Research*, vol. 13, pp. 113-119, 1998.

[4] B. Sen & S. Furber, "Information recovery from rank-order encoded images," *Proceedings of Biologically Inspired Information Fusion*, pp. 8-13, August 2006.

[5] V. Petrovic & C. Xydeas, "Objective evaluation of signal-level image fusion performance," *Optical Engineering*, vol. 14, no. 8, pp. 1-8, 2005.

[6] B. Sen & S. Furber, "Maximising information recovery from rank-order codes," *Proceedings of SPIE Defence Security Symposium*, vol. 6570, pp. 1-12, April 2007.

[7] L. Perrinet et al., "Coding static natural images using spiking event times: do neurons cooperate?," *IEEE Transactions on Neural Networks*, vol. 15, pp. 1164-1175, 2004.

[8] B. Sen, "Information recovery from rank-order encoded images," Chapter 7, pp. 124-140, *PhD. Thesis, University of Manchester, UK* (`http://intranet.cs.man.ac.uk/apt/publications/thesis/Sen08_phd.php`), March 2008.

[9] H. Wassle & B. B. Boycott, "Functional architecture of the mammalian retina," *Physiological Reviews*, vol. 71, no. 2, pp. 447-480, 1991.

[10] V. H. Perry & A. Cowey, "Ganglion cell and cone distribution in the monkey retina," *Vision Research*, vol. 25, no. 12, pp. 1795-1810, 1985.

[11] D. M. Dacey, "The mosaic of midget ganglion cells in the human retina," *The Journal of Neuroscience*, vol. 13, no. 12, pp. 5334-5355, 1993.

[12] H. Wassle, "Parallel processing in the mammalian retina," *Neuroscience*, vol. 5, pp. 1-10, 2004.

[13] H. Kolb, "How the retina works," *American Scientist*, vol. 91, pp. 28-35, 2003.

[14] H. Wassle et al., "Retinal ganglion cell density and cortical magnification factor in the primate," *Vision Research*, vol. 30, no. 11, pp. 1897-1911, 1990.

[15] C. A. Curcio & K. A. Allen, "Topography of ganglion cells in human retina," *The Journal of Comparative Neurology*, vol. 300, pp. 5-25, 1990.

[16] Z. Popovic & J. Sjostrand, "Resolution, separation of retinal ganglion cells, and cortical magnification in humans," *Vision Research*, vol. 41, pp. 1313-1319, 2001.

[17] H. Kolb et al., "Organisation of the retina and visual system," `http://webvision.med.utah.edu/`, 2005.

[18] D. R. Williams, "Seeing through the photoreceptor mosaic," *Trends in Neuroscience*, vol. 9, pp. 193-198, 1986.

[19] D. M. Dacey & M. R. Peterson, "Dendritic field size and morphology of midget and parasol ganglion cells of the human retina," *Proceedings of the National Academy of Sciences of the USA*, vol. 89, pp. 9666-9670, 1992.

[20] J. Sjostrand et al., "Quantitative estimations of foveal and extra-foveal retinal circuitry in humans," *Vision Research*, vol. 39, pp. 2987-2998, 1999.

[21] J. Sjostrand et al., "How many ganglion cells are there to a foveal cone?," *Graefs Archives of Clinical and Experimental Opthalmology*, vol. 232, no. 7, pp. 432-437, 1994.

[22] B. G. Cleland et al., "Physiological identification of a morphological class of cat retinal ganglion cells," *Journal of Physiology*, vol. 248, pp. 151-171, 1975.

[23] H. Kolb & D. Marshak, "The midget pathways of the primate retina," *Documenta Ophthalmologica*, vol. 106, pp. 67-81, 2003.

[24] L. J. Croner & E. Kaplan, "Receptive fields of P and M ganglion cells across the primate retina," *Vision Research*, vol. 35, no. 1, pp. 7-24, 1995.

[25] R. W. Rodieck, "Quantitative Analysis of Cat Retinal Ganglion Cell Response to Visual Stimuli," *Vision Research*, vol. 5, pp. 583-601, 1965.

[26] V. Petrovic, "Subjective Tests for Image Fusion Evaluation and Objective Metric Validation," *Information Fusion*, vol. 8, no. 2, pp. 208-216, 2007.

[27] H. B. Barlow, “Possible Principles Underlying the Transformation of Sensory Messages,” *Sensory Communications*, ed. W. A. Rosenblith, MIT press, pp. 217-234, 1961.
[28] D. J. Field, “What is the goal of sensory coding,” *Neural Computation*, vol. 6, pp. 559-601, 1994.
[29] B. A. Olshausen & D. J. Field, “Natural image statistics and efficient coding,” *Network: computation in neural systems*, vol. 7, pp. 333-339, 1996.
[30] H. K. Hartline et al., “Inhibition in the eye of limulus,” *Journal of General Physiology*, vol. 39, pp. 651-673, 1956.
[31] H. B. Barlow, “Three Points About Lateral Inhibition,” *Sensory Communications*, ed. W. A. Rosenblith, MIT press, pp. 782-786, 1961.
[32] F. Ratliff, “Inhibitory Interaction and the Detection and Enhancement of Contours,” *Sensory Communications*, ed. W. A. Rosenblith, MIT press, pp. 183-203, 1961.